JOC The Journal of Organic Chemistry

Article

pubs.acs.org/joc

Mesolysis Mechanisms of Aromatic Thioether Radical Anions Studied by Pulse Radiolysis and DFT Calculations

Minoru Yamaji,*[,†] Sachiko Tojo,[‡] Mamoru Fujitsuka,[‡] Akira Sugimoto,[‡] and Tetsuro Majima*[,‡]

[†]Division of Molecular Science, Graduate School of Science and Engineering, Gunma University, Kiryu, Gunma 376-8515, Japan

[‡]The Institute of Scientific and Industrial Research (SANKEN), Osaka University, Ibaraki, Osaka 567-0047, Japan

Supporting Information

ABSTRACT: The mesolysis mechanisms for eight aromatic thioether radical anions ($ArCH_2SAr'^{\bullet-}$) generated during radiolysis in 2-methyltetrahydrofuran were studied by spectroscopic measurements and DFT calculation. Seven of $ArCH_2SAr'^{\bullet-}$ underwent mesolysis via dissociation of the σ-bond between the benzylic carbon and sulfur atoms, forming the corresponding radical and anion with the stepwise mechanism or concerted mechanism. Conversely, no mesolysis in the benzyl β-naphthyl sulfide radical anion was found. From the Arrhenius analysis of the mesolysis with the stepwise mechanism, apparent activation energies (ΔE_{exp}) were determined and compared with those (ΔE_{cal}) estimated by the DFT calculations. Two types of C−S bond dissociation are possible to give the C radical and S anion ($ArCH_2^{\bullet}/Ar'S^{-}$) and the C anion and S radical ($ArCH_2^{-}/Ar'S^{\bullet}$). The dissociation energies (BDE($ArCH_2^{\bullet}/Ar'S^{-}$) and BDE($ArCH_2^{-}/Ar'S^{\bullet}$)) were estimated by the DFT calculations, and BDE($ArCH_2^{\bullet}/Ar'S^{-}$) were found to be smaller than BDE($ArCH_2^{-}/Ar'S^{\bullet}$). The formation of $ArCH_2^{\bullet}/Ar'S^{-}$ was observed on the mesolysis of five $ArCH_2SAr'^{\bullet-}$, while one $ArCH_2SAr'^{\bullet-}$ provided $ArCH_2^{-}/Ar'S^{\bullet}$. Chemical properties governing the mesolysis mechanisms of $ArCH_2SAr'^{\bullet-}$ are discussed.

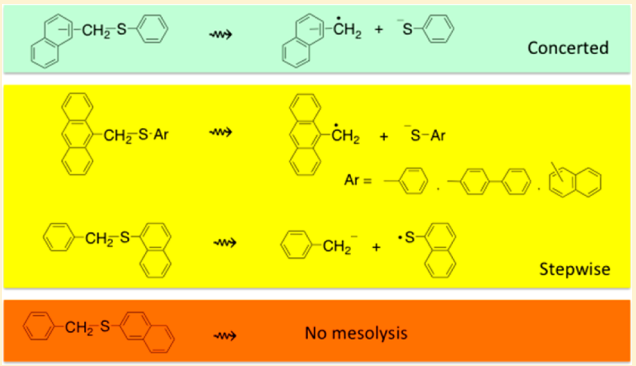

INTRODUCTION

Radical ions are important intermediates for understanding the concept of reaction mechanism in modern organic chemistry.[1] They are produced via one-electron attachment or detachment to the parent neutral molecules, such as photoinduced electron transfer between interacting substrates having well-defined redox potential differences.[2−4] In some molecules having two aromatic groups linked with a σ-bond, intramolecular electron transfer causes the σ-bond dissociation (dissociative electron transfer) as a mesolysis.[5−7] In a recent review, it was shown that mesolysis plays a major role in controlling the chemoselectivity and efficiency of various redox processes.[8] Understanding the mesolysis mechanism is, therefore, crucial toward designing chemical reactions involving electron transfer and bond dissociation. Experimental methodologies for producing radical ions are few. Radiolysis of water and organic solvents is capable of generating strong oxidizing and reducing agents toward the solutes, yielding solute radical ions.[9−16] Pico- and nanosecond transient absorption measurements during pulse radiolysis provide kinetic and mechanistic information on formation and decay of the intermediates.[13,17,18]

Mesolysis promoted by reductive electron transfer to a molecule AB with A and B groups linked by a σ-bond may be subjected to different mesolysis mechanisms.[5−7] One is the concerted mechanism where the electron attachment on AB occurs together with dissociation to A radical ($A^{\bullet}$) and B anion (B^{-}). The other is the stepwise mechanism where the AB radical anion ($AB^{\bullet-}$) is produced on the electron attachment to AB, yielding $A^{\bullet}$ and B^{-}. Scheme 1 illustrates two mesolysis mechanisms.

Scheme 1. Two Mesolysis Mechanisms on One-Electron Reductive Elimination of AB

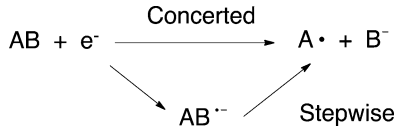

In a previous paper, we reported mesolysis of α,α'-dinaphthyl disulfide ($^{\alpha}NpSSNp^{\alpha}$) in 2-methyltetrahydrofuran (MTHF) using radiolysis techniques.[19] Formation of the $^{\alpha}NpSSNp^{\alpha}$ radical anion ($^{\alpha}NpSSNp^{\alpha\bullet-}$) was observed in a MTHF rigid matrix at 77 K and in fluid MTHF at low temperatures, followed by the mesolysis resulting in the formation of $^{\alpha}NpS^{\bullet}$ + $^{-}SNp^{\alpha}$. The decay kinetics of $^{\alpha}NpSSNp^{\alpha\bullet-}$ obeyed to an Arrhenius expression from which the activation energy and frequency factor were determined for the mesolysis. Generation

Received: April 6, 2015
Published: July 28, 2015

DOI: 10.1021/acs.joc.5b00660
J. Org. Chem. 2015, 80, 7890−7895

of $AB^{\bullet-}$ by radiolysis of AB in MTHF is well understood according to eqs 1 and 2[20]

$$MTHF \rightsquigarrow MTHF^{\cdot+} + e_s^- \quad (1)$$

$$AB + e_s^- \rightarrow AB^{\bullet-} \quad (2)$$

where $MTHF^{\bullet+}$ and e_s^- represent MTHF radical cation and solvated electron, respectively. In the present work, mesolysis of thioethers ($ArCH_2SAr'$) having various aromatic groups (Ar, Ar′) (Chart 1) was investigated by γ-ray radiolysis in the MTHF rigid matrix at 77 K and pulse radiolysis in MTHF at various temperatures. Kinetic analysis for the mesolysis of some $ArCH_2SAr'^{\bullet-}$ provides apparent energy barriers for the mesolysis via the stepwise mechanism. The concerted mechanism is operative for some $ArCH_2SAr'^{\bullet-}$. State energies of radical anions are estimated by the density functional theory (DFT) calculation for drawing the dissociation potential surfaces as a function of the C−S bond distance.

Chart 1. Molecular Structures and Abbreviations of Aromatic Thioethers ($ArCH_2SAr'$) Used in This Work

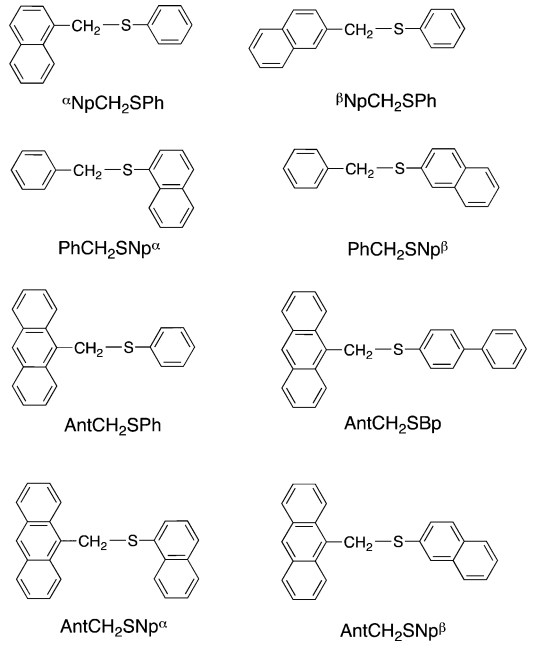

RESULTS

Mesolysis via Stepwise Mechanism. Absorption spectrum observed during the γ-ray radiolysis of $AntCH_2SBp$ in MTHF rigid matrix at 77 K is shown in Figure 1.

The absorption spectrum observed at 77 K is attributable to $AntCH_2SBp^{\bullet-}$ as a stable intermediate. The absorption spectrum having a peak at 670 nm resembles that of the anthracene$^{\bullet-}$,[21] indicating that the electron attached on $AntCH_2SBp^{\bullet-}$ is localized on the anthracene (Ant) moiety. In MTHF at 180 K, the absorption of $AntCH_2SBp^{\bullet-}$ at 670 nm is seen at 50 ns after a 8 ns electron pulse (Figure 1b). With a lapse of time, the absorption decayed showing an isosbestic point at 435 nm with a first-order rate constant, $k_d(670)$ of 2.4×10^6 s^{-1} providing an absorption peak at 420 nm with the same rate (see the insets in Figure 1b). The absorption spectrum at 2.5 μs was similar to that of the 9-anthrylmethyl radical ($AntCH_2^{\bullet}$) as shown in Figure 1c. From the absorption

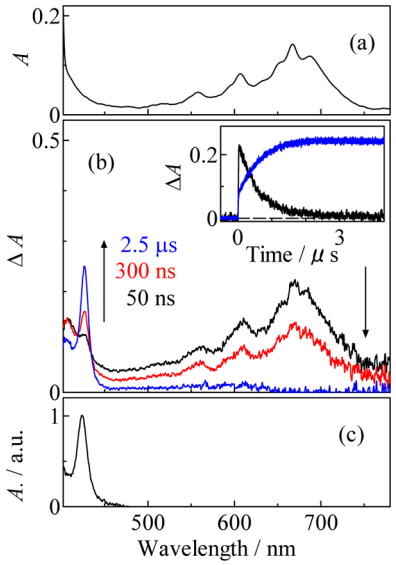

Figure 1. (a) Absorption spectrum observed after the γ-ray radiolysis of $AntCH_2SBp$ in MTHF at 77 K. (b) Time-resolved absorption spectra observed during a 8 ns electron pulse radiolysis of $AntCH_2SBp$ (3 mmol dm^{-3}) in MTHF at 180 K. Inset: time profiles of the absorbance at 670 nm (solid) for $AntCH_2SBp^{\bullet-}$ and at 420 nm (blue) for $AntCH_2^{\bullet}$. (c) Reference absorption spectrum of $AntCH_2^{\bullet}$ in acetonitrile.

spectral changes in Figure 1b, it can be inferred that $AntCH_2SBp^{\bullet-}$ undergoes mesolysis, giving $AntCH_2^{\bullet}$ (Scheme 2).

p-Phenylthiophenolate anion (BpS^-) as the counter fragment of $AntCH_2^{\bullet}$ was not seen in the 400−800 nm wavelength region since its absorption peak is probably located in a shorter wavelength region than 330 nm. These results are also evident for the stepwise mechanism being operative on the mesolysis of $AntCH_2SBp^{\bullet-}$.

Temperature dependence of the decay rate constant, $k_d(670)$, of $AntCH_2SBp^{\bullet-}$ leading to the formation of $AntCH_2^{\bullet}$ and BpS^- was examined in a temperature range of 160−220 K. Figure 2 shows the Arrhenius plot of $k_d(670)$.

The plot of $k_d(670)$ vs T^{-1} gave a straight line according to the Arrhenius equation

$$\ln k_d(670) = \ln A - \Delta E_{exp}(RT)^{-1} \quad (3)$$

where A and ΔE_{exp} denote a frequency factor and an apparent activation energy for the mesolysis of $AntCH_2SBp^{\bullet-}$, respectively. From the slope and intercept of the line, ΔE_{exp} and A for mesolysis of $AntCH_2SBp^{\bullet-}$ were determined to be 4.6 kcal mol^{-1} and 6.1×10^{11} s^{-1}, respectively. Formation of the corresponding $ArCH_2SAr'^{\bullet-}$ was also seen during the pulse radiolysis of $AntCH_2SNp^{\alpha}$, $AntCH_2SNp^{\beta}$, $AntCH_2SPh$, and $PhCH_2SNp^{\alpha}$ in MTHF, followed by yielding the corresponding radical and anion via the mesolysis. Consequently, the stepwise mechanism governs the mesolysis of $AntCH_2SAr'^{\bullet-}$ and $PhCH_2SNp^{\alpha\bullet-}$. Their absorption spectral data and Arrhenius plots are deposited in the Supporting Information (Figures S1−4), whereas ΔE_{exp} and A for the mesolysis of $ArCH_2SAr'^{\bullet-}$ are listed in Table 1. Interestingly, $PhCH_2SNp^{\alpha\bullet-}$ dissociates into $PhCH_2^-$ and $Np^{\alpha}S^{\bullet}$, while $AntCH_2SAr'^{\bullet-}$ dissociate into $AntCH_2^{\bullet}$ and thiolate anions ($Ar'S^-$).

Mesolysis via the Concerted Mechanism. Absorption spectral changes observed after the γ-ray radiolysis of

DOI: 10.1021/acs.joc.5b00660
J. Org. Chem. 2015, 80, 7890−7895

Scheme 2. Mesolysis of $AntCH_2SBp^{\bullet-}$ via the Stepwise Mechanism

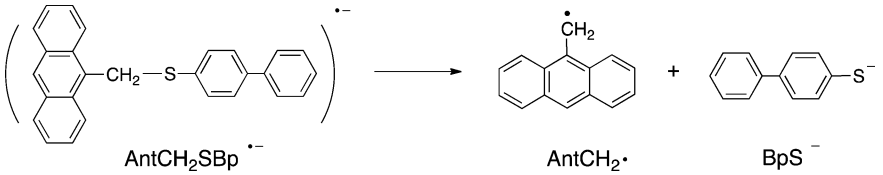

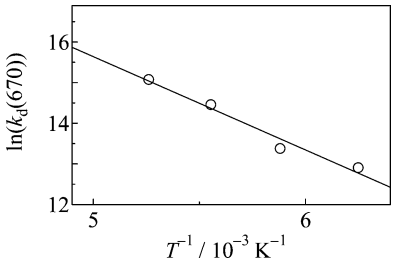

Figure 2. Arrhenius plots of the decay rate constant, $k_d(670)$, of the transient absorption at 670 nm for $AntCH_2SBp^{\bullet-}$.

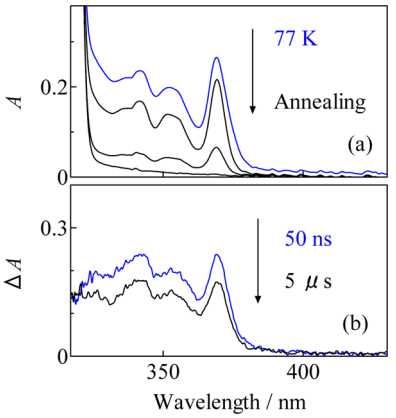

Figure 3. (a) Absorption spectral changes upon annealing from 77 to 295 K after the γ-radiolysis of $^{\alpha}NpCH_2SPh$ (3 mmol dm^{-3}) in MTHF rigid matrix at 77 K for 60 min. (b) Transient absorption spectra observed after a 8 ns electron pulse during the pulse radiolysis of $^{\alpha}NpCH_2SPh$ in the MTHF solution at 200 K.

$^{\alpha}NpCH_2SPh$ in MTHF at 77 K upon annealing from 77 to 295 K are represented in Figure 3a.

The absorption peaks at 330−380 nm are due to the α-naphthylmethyl radical ($^{\alpha}NpCH_2^{\bullet}$).[22] $^{\alpha}NpCH_2SPh^{\bullet-}$ with absorption peaks at 380 and 770 nm[21] was not observed in the transient absorption spectra, indicating that $^{\alpha}NpCH_2SPh^{\bullet-}$ has a lifetime shorter than 50 ns. As temperatures of the matrix increase, the absorption spectrum for $^{\alpha}NpCH_2^{\bullet}$ decayed. In MTHF at 200 K, the absorption peaks of $^{\alpha}NpCH_2^{\bullet}$ were seen at 50 ns after a 8 ns electron pulse during the pulse radiolysis (Figure 3b). With a lapse of time, the absorption peaks decayed. From these observations, it is indicated that the concerted mechanism is operative for the decomposition of $^{\alpha}NpCH_2SPh$ upon one-electron reduction (Scheme 3).

Formation of the absorption peaks due to β-methylnaphthyl radical ($^{\beta}NpCH_2^{\bullet}$) was seen during a 8 ns electron pulse radiolysis of −$NpCH_2SPh$ in MTHF at low temperatures. The absorption spectral data are deposited in the Supporting Information (Figure S5).

No Mesolysis in $PhCH_2SNp^{\beta\bullet-}$. During the radiolysis of $PhCH_2SNp^{\beta}$ in MTHF, we found no mesolysis of $PhCH_2SNp^{\beta\bullet-}$. Absorption spectral changes observed after the γ-ray radiolysis of $PhCH_2SNp^{\beta}$ in MTHF at 77 K upon annealing from 77 to 295 K are represented in Figure 4a.

Scheme 3. Mesolysis of $^{\alpha}NpCH_2SPh$ via the Concerted Mechanism

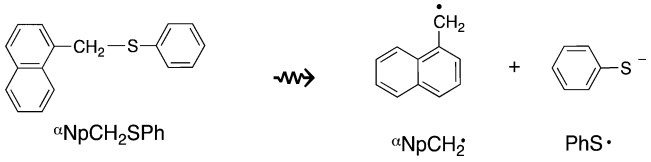

The absorption peak at 425 nm at 77 K ascribable to $PhCH_2SNp^{\beta\bullet-}$ diminished with a blue shift giving no appreciable absorption in the wavelength region longer than 350 nm with increasing temperature from 77 K to room temperature. The shape of the absorption spectrum observed at 50 ns after a 8 ns electron pulse radiolysis of $PhCH_2SNp^{\beta}$ in MTHF at 180 K (Figure 4b) resembles that of $PhCH_2SNp^{\beta\bullet-}$ in Figure 4a. With a lapse of time from 50 ns to 1 μs, the

Table 1. Frequency Factors (A), Activation Energies (ΔE_{exp} and ΔE_{cal}), Bond Dissociation Energies (BDE), and Mesolysis Mechanism for $ArCH_2SAr'^{\bullet-}$

compd	A (s^{-1})	ΔE_{exp}[a] (kcal mol^{-1})	ΔE_{cal}[b] (kcal mol^{-1})	BDE($ArCH_2^{\bullet}/Ar'S^{-}$) (kcal mol^{-1})	BDE($ArCH_2^{-}/Ar'S^{\bullet}$) (kcal mol^{-1})	mechanism[c]
$PhCH_2SNp^{\alpha}$	1.6×10^9	2.2	~0	−14.2	25.1[d]	S/W
$PhCH_2SNp^{\beta}$			~0	−15.5	37.4	no
$^{\alpha}NpCH_2SPh$	N/A	N/A	*e*	1.4[d]	48.5	conc
$^{\beta}NpCH_2SPh$	N/A	N/A	*e*	1.0[d]	47.8	conc
$AntCH_2SPh$	2.4×10^{12}	5.6	1.7	−8.0[d]	33.7	S/W
$AntCH_2SBp$	6.1×10^{11}	4.6	*e*	−7.9[d]	22.1	S/W
$AntCH_2SNp^{\alpha}$	3.6×10^{12}	4.9	*e*	−9.1[d]	20.4	S/W
$AntCH_2SNp^{\beta}$	1.2×10^{12}	4.8	2.1	−8.7[d]	34.4	S/W

[a]Obtained from the Arrhenius analysis of $ArCH_2SAr'^{\bullet-}$ decay rates. [b]The difference between the minimal and the maximal of state energies of $ArCH_2SAr'^{\bullet-}$ estimated by the DFT calculation. [c]S/W and conc are abbreviated for the stepwise and concerted mechanisms, respectively. "No" indicates the absence of mesolysis. [d]Applicable to the actual formation of the radical and the anion. [e]Not obtained.

DOI: 10.1021/acs.joc.5b00660
J. Org. Chem. 2015, 80, 7890−7895

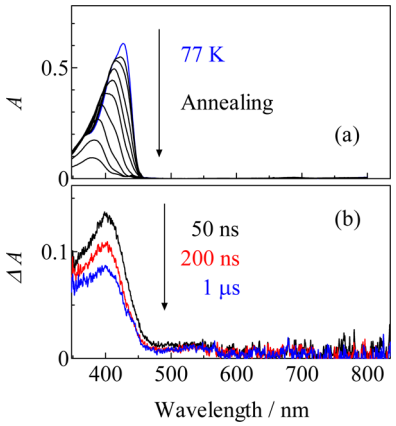

Figure 4. (a) Absorption spectral changes on annealing from 77 to 295 K after the γ-radiolysis of $PhCH_2SNp^{\beta}$ (3 mmol dm^{-3}) in MTHF rigid matrix at 77 K for 60 min. (b) Absorption spectral changes observed after a 8 ns electron pulse during the pulse radiolysis of $PhCH_2SNp^{\beta}$ in MTHF at 180 K.

absorption peak of $PhCH_2SNp^{\beta\bullet-}$ at 400 nm decreased without a wavelength shift. On the decrease of $PhCH_2SNp^{\beta\bullet-}$, no absorption peaks, such as β-naphthylthiyl radical ($^{\beta}$Np S$^{\bullet}$),[23] evolved in the wavelength longer than 350 nm. From these observations, we concluded that no mesolysis occurs in $PhCH_2SNp^{\beta\bullet-}$.

Mesolysis Mechanism and Bond Dissociation Energies by DFT Calculation. State energies (ΔE^{RA}) of $ArCH_2SAr'^{\bullet-}$ were estimated by the DFT calculations at the UB3LYP/6-31G(d) level. The state energies (ΔE^{RA}) as a function of the C−S bond distance, r(C−S), are represented in Figure 5.

As r(C−S) increases, ΔE^{RA} for $PhCH_2SNp^{\bullet-}$ uniformly decreases, which is characteristic for the concerted mechanism. As for $AntCH_2SPh^{\bullet-}$ and $AntCH_2SNp^{\beta\bullet-}$, the minimum and maximum values were clearly seen on ΔE^{RA}. The energy

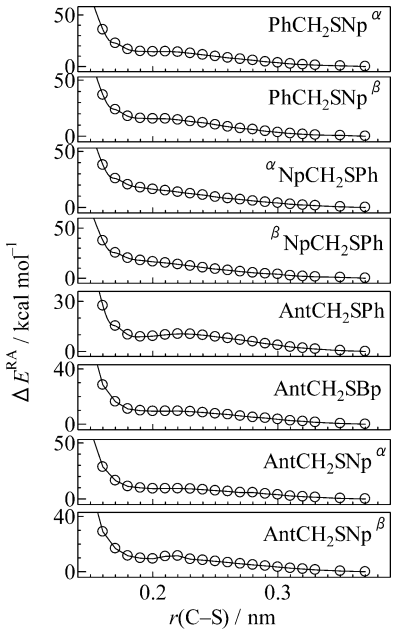

Figure 5. State energies of $ArCH_2SAr'^{\bullet-}$ calculated at the UB3LYP/6-31G(d) level considering the dielectric constant of THF.

differences between the minimal and maximal values are calculated to be activation energies for the mesolysis (ΔE_{cal}). The positive ΔE_{cal} for $AntCH_2SPh^{\bullet-}$ and $AntCH_2SNp^{\beta\bullet-}$ indicate that these $ArCH_2SAr'^{\bullet-}$ have definite lifetimes for the mesolysis on the stepwise mechanism. ΔE_{cal} for $PhCH_2SNp^{\bullet-}$ was close to zero (Table 1).

Bond dissociation energies (BDE) of the benzylic C−S bond of $ArCH_2SAr'^{\bullet-}$ can be estimated according to eq 4

$$\Delta H_f(RA) = \Delta H_f(R) + \Delta H_f(A) - BDE \quad (4)$$

where ΔH_f(RA), ΔH_f(R), and ΔH_f(A) denote the formation heat of $ArCH_2SAr'^{\bullet-}$ (RA), radical (R), and anion (A), respectively. ΔH_f(RA), ΔH_f(R), and ΔH_f(A) calculated by DFT calculations using UB3LYP at the 6-31G(d) level are deposited in the Supporting Information (Tables S1 and 2). For the mesolysis of $ArCH_2SAr'^{\bullet-}$, two BDE are calculated for the formation of $ArCH_2^{\bullet}/Ar'S^{-}$ and $ArCH_2^{-}/Ar'S^{\bullet}$ (Table 1). $ArCH_2^{\bullet}/Ar'S^{-}$ were produced in the mesolysis of $AntCH_2SAr'^{\bullet-}$ and $NpCH_2SPh^{\bullet-}$, while $ArCH_2^{-}/Ar'S^{\bullet}$ was produced for $PhCH_2SNp^{\alpha\bullet-}$. It is noteworthy that BDE($ArCH_2^{\bullet}/Ar'S^{-}$) are smaller than BDE($ArCH_2^{-}/Ar'S^{\bullet}$).

DISCUSSION

In the present work, mesolysis mechanisms of $ArCH_2SAr'^{\bullet-}$ via the stepwise or concerted mechanisms are examined. All $AntCH_2SAr'^{\bullet-}$ undergo mesolysis via the stepwise mechanism. The apparent activation energies, ΔE_{exp}, obtained from the Arrhenius plots are as large as ca. 5.0 kcal mol^{-1} and larger than those (ΔE_{cal}) estimated by the DFT calculations (~2.0 kcal mol^{-1}). For $AntCH_2SBP^{\bullet-}$ and $AntCH_2SNp^{\alpha\bullet-}$, definite ΔE_{cal} were not obtained. Moreover, the absence of ΔE_{cal} for $NpCH_2SPh^{\bullet-}$ suggests that the mesolysis is governed by the concerted mechanism. No mesolysis was observed for $PhCH_2SNp^{\beta\bullet-}$, although the potential surface of ΔE^{RA} predicts the mesolysis via the concerted mechanism. Next, we elucidate the relationship between the calculated BDE and the mesolytic features. The calculated BDE values for the $ArCH_2^{\bullet}/Ar'S^{-}$ formation are greater than those for the $ArCH_2^{-}/Ar'S^{\bullet}$ formation. From an energetic viewpoint, mesolysis of $ArCH_2SAr'^{\bullet-}$ forms the $ArCH_2^{\bullet}/Ar'S^{-}$ type intermediates. We have obtained that $NpCH_2SPh^{\bullet-}$ subjected to the concerted mesolysis have small positive BDE values for the $ArCH_2^{\bullet}/Ar'S^{-}$ formation in contrast to negative ones of the other thioethers preferring stepwise mesolysis. This finding would provide a criterion that the calculated BDE values for the $ArCH_2^{\bullet}/Ar'S^{-}$ formation may predict the mesolysis mechanism. The calculated negative BDEs for $ArCH_2^{\bullet}/Ar'S^{-}$ indicate that the C−S bond in the corresponding $ArCH_2SAr'^{\bullet-}$ is dissociative in nature. However, $PhCH_2SNp^{\bullet-}$ having BDE of ca. −15 kcal mol^{-1} for $ArCH_2^{\bullet}/Ar'S^{-}$ are exceptional. No C−S bond cleavage in $PhCH_2SNp^{\beta\bullet-}$ was observed whereas the formation of $^{\alpha}$NpS$^{\bullet}$ and $PhCH_2^{-}$ was seen on the mesolysis of $PhCH_2SNp^{\alpha\bullet-}$. The calculated BDE($ArCH_2^{-}/Ar'S^{\bullet}$) (25.1 kcal mol^{-1}) for $PhCH_2SNp^{\alpha\bullet-}$ is substantially greater than the BDE($ArCH_2^{\bullet}/Ar'S^{-}$) (−14.2 kcal mol^{-1}). From the energetic viewpoint, the mesolysis of $PhCH_2SNp^{\alpha\bullet-}$ is much endothermic compared to those of $AntCH_2SAr'^{\bullet-}$.

$ArCH_2SAr'^{\bullet-}$ are three-electron-bonded radicals where the C−S σ−bonding molecular orbital is occupied by two electrons, and the C−S antibonding σ* orbital is singly occupied. The orbital occupation between the benzylic carbon and sulfur atoms is expressed as $\sigma(2)\sigma^*(1)$. The antibonding σ* electron is responsible for the bond weakening and facile

DOI: 10.1021/acs.joc.5b00660
J. Org. Chem. 2015, 80, 7890−7895

bond dissociation. The concerted mechanism for the reductive dissociation of the C−S bond of $ArCH_2SAr'^{\bullet-}$ is interpreted by considering a direct occupation of the attached electron on the σ^* orbital of $NpCH_2SPh$. Conversely, for the stepwise mechanism, $ArCH_2SAr'^{\bullet-}$ having definite lifetimes undergo mesolysis with definite activation energies. The absorption spectral shapes of $AntCH_2SAr'^{\bullet-}$ and $PhCH_2SNp^{\alpha\bullet-}$ are similar to those of radical anions of anthracene and naphthalene thiols, respectively.[21] These results indicate the attached electron is localized on the larger aromatic group in $ArCH_2SAr'^{\bullet-}$. The captured electron intramolecularly moves from the aromatic group to the σ^* orbital during the molecular motion, which may affect A and ΔE_{exp}.

CONCLUSIONS

The mesolysis mechanisms of $ArCH_2SAr'^{\bullet-}$ generated in MTHF have been investigated on the basis of the absorption measurements and DFT calculations. Mesolysis of $NpCH_2SPh^{\bullet-}$ (C−S bond dissociation) occurs via the concerted mechanism, while no mesolysis of $PhCH_2SNp^{\beta\bullet-}$ is found. Mesolyses of $AntCH_2SAr'^{\bullet-}$ and $PhCH_2SNp^{\alpha\bullet-}$ occur via the stepwise mechanism, yielding $AntCH_2^{\bullet}/Ar'S^-$ and $PhCH_2^-/{}^{\alpha}NpS^{\bullet}$, respectively. On the basis of the Arrhenius analysis for the decay kinetics of $ArCH_2SAr'^{\bullet-}$, ΔE_{exp} and A were determined to be compared with ΔE_{cal} estimated by the DFT calculation. $BDE(ArCH_2^{\bullet}/Ar'S^-)$ and $BDE(ArCH_2^-/Ar'S^{\bullet})$ were evaluated by the DFT calculations. The former values provide a criterion for the mesolysis mechanism and the positive and negative values for the concerted and stepwise mechanisms, respectively. As for the BDE, $PhCH_2SNp^{\bullet-}$ are exceptional. The mesolysis of $PhCH_2SNp^{\alpha\bullet-}$ provides $ArCH_2^-/Ar'S^{\bullet}$ where $BDE(ArCH_2^-/Ar'S^{\bullet})$ is substantially larger than $BDE(ArCH_2^{\bullet}/Ar'S^-)$. Consequently, the mesolysis mechanism of $ArCH_2SAr'^{\bullet-}$ strongly depends on the varieties of the aromatic groups (Ar and Ar′).

EXPERIMENTAL SECTION

General Synthesis Procedures for $PhCH_2SNp^{\alpha}$, $PhCH2SNp^{\beta}$, ${}^{\alpha}NpCH2SPh$, and ${}^{\beta}NpCH_2SPh$. Aryl thiol (10 mmol) was added to a solution of the corresponding arylmethyl halide (5 mmol) and K_2CO_3 (50 mmol) in 50 mL of acetone. After the reaction mixture was refluxed for 12 h, it was cooled to room temperature and filtrated. After the solvent was evaporated by reduced pressure, the crude product was purified by flash column chromatography using a hexane/chloroform eluent. The NMR data of $PhCH_2SNp^{\alpha}$, $PhCH2SNp^{\beta}$, ${}^{\alpha}NpCH2SPh$, and ${}^{\beta}NpCH_2SPh$ were consistent with those reported previously.[24−26]

General Synthesis Procedures for Anthrylmethyl Sulfides. An acetone (30 mL) solution of 9-(chloromethyl)anthracene (500 mg, 2.2 mmol) and aryl thiol (3.5 mmol) in the presence of K_2CO_3 (1.2 g, 8.7 mmol) was refluxed for 12 h. After being cooled to room temperature, the solution was filtrated, and the solvent was evaporated under reduced pressure. The product was purified by GPC using chloroform eluent and recrystallized from ethanol. Melting points were measured by a Yanaco micro melting point apparatus and uncorrected.

$AntCH_2SPh$. Yield: 80% (530 mg). Colorless leaflet. Mp: 152.5−153 °C. ^1H NMR (400 MHz, $CDCl_3$): δ 8.43 (s, 1H), 8.27 (d, 2H, J = 8.7 Hz), 8.02 (d, 2H, J = 9.2 Hz), 7.54−7.45 (m, 6H), 7.35−7.23 (m, 3H), 5.13 (s, 2H). ^{13}C NMR (100 MHz, $CDCl_3$): δ 131.6, 130.3, 130.0, 129.3, 129.1, 127.9, 127.7, 126.6, 126.4, 125.2, 124.2, 32.2. Anal. Calcd for $C_{21}H_{16}S$: C, 83.96; H, 5.37. Found: C, 83.94; H, 5.45.

$AntCH_2SBp$. Yield: 79% (650 mg). White powder. Mp: 192.5−194 °C. ^1H NMR (400 MHz, $CDCl_3$) δ 8.44 (s, 1H), 8.29 (d, 2H, J = 8.7 Hz), 8.03 (d, 2H, J = 8.2 Hz), 7.61−7.45 (m, 12H), 7.37−7.39 (m, 1H), 5.17 (s, 2H). ^{13}C NMR (100 MHz, $CDCl_3$) δ 131.7, 130.4, 130.3, 129.3, 129.0, 127.9, 127.8, 127.7, 127.5, 127.1, 126.4, 125.2, 124.2, 32.3. Anal. Calcd for $C_{27}H_{20}S$: C, 86.13; H, 5.35. Found: C, 85.95; H, 5.46.

$AntCH_2SNp^{\alpha}$. Yield: 75% (580 mg). Colorless prism. Mp: 200−202 °C. ^1H NMR (400 MHz, $CDCl_3$): δ 8.45−8.43 (m, 2H), 8.22−8.20 (m, 2H), 8.02−7.99 (m, 2H), 7.89−7.85 (m, 1H), 7.78 (d, 1H, J = 8.2 Hz), 7.69 (d, 1H, J = 7.1 Hz), 7.55−7.44 (m, 6H), 7.39 (t, 1H, J = 7.6 Hz), 5.13 (s, 2H). ^{13}C NMR (100 MHz, $CDCl_3$): δ 134.4, 133.9, 133.1, 131.5, 130.2, 129.2, 128.6, 127.9, 127.8, 127.7, 126.5, 126.3, 126.2, 125.7, 125.2, 125.1, 124.1, 32.4. Anal. Calcd for $C_{25}H_{18}S$: C, 85.68; H, 5.18. Found: C, 85.46; H, 5.40.

$AntCH_2SNp^{\beta}$. Yield: 78% (600 mg). Colorless prism. Mp: 173−175 °C. ^1H NMR (400 MHz, $CDCl_3$): δ 8.44 (s, 1H), 8.30 (t, 2H, J = 9.2 Hz), 8.02 (d, 2H, J = 9.2 Hz), 7.93 (s, 1H), 7.84−7.78 (m, 3H), 7.54−7.44 (m, 7H), 5.23 (s, 2H). ^{13}C NMR (100 MHz, $CDCl_3$): δ 135.4, 134.0, 131.7, 130.3, 129.3, 128.6, 128.0, 127.9, 127.7, 127.31, 127.26, 126.8, 126.5, 125.9, 125.2, 124.2, 32.1. Anal. Calcd for $C_{25}H_{18}S$: C, 85.68; H, 5.18. Found: C, 85.49; H, 5.25.

2-Methyltetrahydrofuran (MTHF, Tokyo Kasei) was distilled over CaH_2 before use. MTHF solutions of the compounds were degassed by several freeze−pump−thaw cycles on a high vacuum line (5×10^{-4} Torr) and sealed in a 1 cm path length quartz cell. The concentration of the thioethers was 3×10^{-3} mol dm^{-3} throughout this work.

Instruments. γ-Ray radiolysis was carried out for 30 min with a ^{60}Co source at Osaka University. The dose rate was 4 kGy h^{-1}. Visible absorption spectra after the γ-radiolysis of $ArCH_2SAr'$ in MTHF rigid matrix were recorded on a spectrophotometer (Shimadzu Multispec-1500). Transient absorption spectra were measured during the pulse radiolysis of $ArCH_2SAr'$ in MTHF using a linear accelerator at Osaka University (28 MeV, 8 ns, 0.87 kGy $pulse^{-1}$). The details of the detection system for transient absorption have been described elsewhere.[27] Transient absorption spectra were taken by using a photodiode array (Hamamatsu Photonics, S3904-1024F) with a gated image intensifier (Hamamatsu Photonics, C2925-01) as a detector. The temperature effects were examined using a cryostat (Oxford DN704) with a digital temperature controller (DTC-2) with precision of ±1.0 °C. ^1H and ^{13}C spectra were recorded on an NMR System 400 MHz spectrometer.

The calculation was carried out at the DFT level using the Gaussian 09 software package. The geometries of the thioethers were fully optimized by using the 6-31G(d) base set at the UB3LYP method considering a dielectric constant of tetrahydrofuran in the CPCM model.

ASSOCIATED CONTENT

Supporting Information

The Supporting Information is available free of charge on the ACS Publications website at DOI: 10.1021/acs.joc.5b00660.

Mesolysis profiles of radical anions of $AntCH_2SPh$, $AntCH_2SNp^{\alpha}$, $AntCH_2SNp^{\beta}$, $PhCH_2SNp^{\alpha}$ and ${}^{\beta}NpCH_2SPh$; results of DFT calculation including tables of atom coordinates for the optimized geometries; and ^1H and ^{13}C NMR spectra of $AntCH_2SPh$, $AntCH_2SBp$, $AntCH_2SNp^{\alpha}$, and $AntCH_2SNp^{\beta}$ (PDF)

AUTHOR INFORMATION

Corresponding Authors

*E-mail (M.Y.): yamaji@gunma-u.ac.jp.

*E-Mail (T.M.): majima@sanken.osaka-u.ac.jp.

Notes

The authors declare no competing financial interest.

ACKNOWLEDGMENTS

We thank Dr. Takumi Kimura for performing the experiments and the staff for running the pulse radiolysis facilities in the Radiation Laboratory, The Institute of Scientific and Industrial

DOI: 10.1021/acs.joc.5b00660
J. Org. Chem. 2015, 80, 7890−7895

Research, Osaka University. This work has been partly supported by a Grant-in-Aid for Scientific Research (25220806, 25288035, 25390125, 26288032, and others) from the Ministry of Education, Culture, Sports, Science and Technology (MEXT) of Japanese Government.

REFERENCES

(1) Fujitsuka, M.; Majima, T. *J. Phys. Chem. Lett.* **2011**, *2*, 2965−2971.
(2) Fox, M. A. *Chem. Rev.* **1979**, *79*, 253−273.
(3) Julliard, M.; Chanon, M. *Chem. Rev.* **1983**, *83*, 425−506.
(4) Kavarnos, G. J.; Turro, N. J. *Chem. Rev.* **1986**, *86*, 401−449.
(5) Savéant, J.-M. *Adv. Phys. Org. Chem.* **2000**, *35*, 117−192.
(6) Antonello, S.; Maran, F. *Chem. Soc. Rev.* **2005**, *34*, 418−428.
(7) Costentin, C.; Robert, M.; Savéant, J.-M. *Chem. Phys.* **2006**, *324*, 40−56.
(8) Houmam, A. *Chem. Rev.* **2008**, *108*, 2180−2237.
(9) Tojo, S.; Morishima, K.; Ishida, A.; Majima, T.; Takamuku, S. *J. Org. Chem.* **1995**, *60*, 4684−4685.
(10) Majima, T.; Tojo, S.; Ishida, A.; Takamuku, S. *J. Org. Chem.* **1996**, *61*, 7793−7800.
(11) Tojo, S.; Yasui, S.; Fujitsuka, M.; Majima, T. *J. Org. Chem.* **2006**, *71*, 8227−8232.
(12) Tojo, S.; Fujitsuka, M.; Majima, T. *J. Org. Chem.* **2010**, *75*, 3618−3625.
(13) Fujitsuka, M.; Samori, S.; Tojo, S.; Haley, M. M.; Majima, T. *ChemPlusChem* **2012**, *77*, 682−687.
(14) Tojo, S.; Fujitsuka, M.; Majima, T. *J. Org. Chem.* **2012**, *77*, 4932−4938.
(15) Tojo, S.; Fujitsuka, M.; Majima, T. *J. Org. Chem.* **2013**, *78*, 1887−1893.
(16) Tojo, S.; Fujitsuka, M.; Majima, T. *J. Org. Chem.* **2013**, *78*, 1887−1893.
(17) Saeki, A.; Kozawa, T.; Ohnishi, Y.; Tagawa, S. *J. Phys. Chem. A* **2007**, *111*, 1229−1235.
(18) Higashino, S.; Saeki, A.; Okamoto, K.; Tagawa, S.; Kozawa, T. *J. Phys. Chem. A* **2010**, *114*, 8069−8074.
(19) Yamaji, M.; Tojo, S.; Takehira, K.; Tobita, S.; Fujitsuka, M.; Majima, T. *J. Phys. Chem. A* **2006**, *110*, 13487−13491.
(20) Ichikawa, T.; Yoshida, H.; Hayashi, K. *J. Nucl. Sci. Technol.* **1972**, *9*, 538−543.
(21) Shida, T. *Electronic Absorption Spectra of Radical Ions*; Elsevier: Tokyo, 1988.
(22) Johnston, L. J.; Scaiano, J. C. *J. Am. Chem. Soc.* **1985**, *107*, 6368−6372.
(23) Yamaji, M.; Ueda, S.; Shizuka, H.; Tobita, S. *Phys. Chem. Chem. Phys.* **2001**, *3*, 3102−3106.
(24) Eichman, C. C.; Stambuli, J. P. *J. Org. Chem.* **2009**, *74*, 4005−4008.
(25) Dneprovskii, A. S.; Fedosov, I. V. *Russ. J. Org. Chem.* **2001**, *37*, 1438−1443.
(26) Bryliakov, K. P.; Talsi, E. P. *Eur. J. Org. Chem.* **2011**, *2011*, 4693−4698.
(27) Tachikawa, T.; Tojo, S.; Fujitsuka, M.; Majima, T. *J. Phys. Chem. B* **2005**, *109*, 17460−17466.

DOI: 10.1021/acs.joc.5b00660
J. Org. Chem. 2015, 80, 7890−7895